Modelling the photochemical attenuation pathways of the fibrate drug gemfibrozil in surface waters

Modelling the photochemical attenuation pathways of the fibrate drug gemfibrozil in surface waters

Debora Fabbri,[a] Valter Maurino,[a] Marco Minella,[a] Claudio Minero,[a] Davide Vione [a,b]*

[a] *Università degli Studi di Torino, Dipartimento di Chimica, Via P. Giuria 5, 10125 Torino, Italy. http://www.chimicadellambiente.unito.it*

[b] *Università degli Studi di Torino, Centro Interdipartimentale NatRisk, Via L. Da Vinci 44, 10095 Grugliasco (TO), Italy. http://www.natrisk.org*

* Corresponding author. Phone +39-011-6705296; Fax +39-011-6705242; E-mail: *davide.vione@unito.it*

Abstract

Gemfibrozil (GFZ) is a relatively persistent pollutant in surface-water environments and it is rather recalcitrant to biological degradation. The GFZ photochemical lifetimes are relatively short in shallow waters with low levels of dissolved organic carbon (DOC), but they can reach the month-year range in deep and high-DOC waters. The main reason is that GFZ undergoes negligible reaction with singlet oxygen or degradation sensitised by the triplet states of chromophoric dissolved organic matter, which are the usually prevalent photochemical pathways in deep and high-DOC sunlit waters. Nitrate and nitrite scarcely affect the overall GFZ lifetimes, but they can shift photodegradation from direct photolysis to the $^{\bullet}OH$ process. These two pathways are the main GFZ phototransformation routes, with the direct photolysis prevailing in shallow environments

during summer. Under these conditions the GFZ photochemical lifetimes are also shorter and the environmental significance of photodegradation correspondingly higher. The direct photolysis of GFZ under UVB irradiation yielded several transformation intermediates deriving from oxidation or cleavage of the aliphatic lateral chain. A quinone derivative (2,5-dimethyl-1,4-benzoquinone), a likely oxidation product of the transformation intermediate 2,5-dimethylphenol, is expected to be the most acutely and chronically toxic compound arsing from GFZ direct photolysis. Interestingly, literature evidence suggests that the same toxic intermediate would be formed upon $^{\bullet}$OH reaction.

Keywords: Gemfibrozil; Environmental Photochemistry; Direct Photolysis; Transformation Intermediates; Emerging Pollutants.

1. Introduction

Gemfibrozil (GFZ) is a lipid regulator that belongs to the class of fibrate drugs. It is widely used, with an estimated 2.2 million prescriptions per year and over 350 million $ sales volume in the US only in 2013 (HealthGrove, 2016). This compound is incompletely removed from wastewater during treatment and it can be found in treated wastewater at μg L^{-1} levels (Andreozzi et al., 2003), as well as in surface waters at ng L^{-1} levels (Osorio et al., 2016). Out of 55 screened pharmaceuticals, GFZ was the main contributor to toxic units (TU, calculated as the ratio between the detected concentration and the EC50 value) for fish and the second largest contributor for crustaceans in Iberian rivers (Osorio et al., 2016).

There is evidence that GFZ is recalcitrant to biodegradation (coherently with its incomplete removal in wastewater treatment; D'Alessio et al., 2015), however it can undergo phototransformation under environmentally significant irradiation conditions (Ma et al., 2016). The phototransformation of

GFZ by direct photolysis and indirect photochemistry might thus play an important role in surface-water environments. Coherently, Araujo et al. (2011) have shown that GFZ photochemistry can prevail over biodegradation, but the estimated photochemical half-life times in surface-water samples can reach up to over 200 days under real sunlight. Therefore, GFZ is predicted to be a fairly persistent pollutant in surface waters.

The photochemical degradation processes of xenobiotics in sunlit waters consist of a series of different reaction pathways, which involve direct photolysis following sunlight absorption by the substrate and indirect photochemistry, triggered by reaction with photogenerated transient species (Boreen et al., 2003). The radicals $^{\bullet}OH$ and $CO_3^{-\bullet}$, singlet oxygen ($^1O_2$) and the triplet states of chromophoric dissolved organic matter (^{3}CDOM*) are among the most important photoinduced transients. They are photochemically produced upon sunlight absorption by photosensitisers such as chromophoric dissolved organic matter (CDOM), nitrate and nitrite (Vione et al., 2014). CDOM is beyond doubt the main photosensitiser in surface waters because it is the only source of ^{3}CDOM* and $^1O_2$, and it is also a major source of $^{\bullet}OH$. Anyway, the details of the photoreaction pathways leading to $^{\bullet}OH$ photoproduction by irradiated CDOM are still largely missing (Page et al., 2011; Gligorovski et al., 2015). CDOM is also a key actor in the formation of $CO_3^{-\bullet}$ through reaction of CDOM-photogenerated $^{\bullet}OH$ with carbonate and bicarbonate. The oxidation of carbonate by ^{3}CDOM* is a further $CO_3^{-\bullet}$ source, particularly in surface waters with elevated values of dissolved organic carbon (DOC) and pH (Canonica et al., 2005). Moreover, dissolved organic matter (DOM, not necessarily chromophoric) is the main scavenger of $^{\bullet}OH$ and most notably of $CO_3^{-\bullet}$. Because, on the contrary, DOM does not scavenge ^{3}CDOM* or $^1O_2$ significantly (Wenk et al., 2013), the reactions with $CO_3^{-\bullet}$ are usually favoured in low-DOC waters, while the $^{\bullet}OH$ processes and the direct photolysis might be important in the presence of intermediate DOC values. Finally, the reactions with $^1O_2$ and ^{3}CDOM* generally prevail in high-DOC environments (Vione et al., 2014).

The goal of the present paper is to assess the photochemical GFZ lifetimes and the importance of GFZ phototransformation pathways under conditions that are significant to surface waters, modelling the different direct and indirect GFZ phototransformation pathways as a function of water chemistry, depth and season, on the basis of the known photoreactivity parameters.

2. Methods

The photodegradation of GFZ was assessed with the APEX software (Aqueous Photochemistry of Environmentally-occurring Xenobiotics; Bodrato and Vione, 2014), which predicts photochemical reaction kinetics from photoreactivity parameters (absorption spectra, direct photolysis quantum yields and second-order reaction rate constants with photoinduced transients), from data of water chemistry and depth, and from sunlight irradiance and spectrum (Frank and Klöpffer, 1988). The available GFZ photoreactivity parameters are reported in **Table 1**, and the GFZ absorption spectrum in **Figure SM1** of the Supplementary Material (hereafter SM). No data are available for the reaction kinetics between GFZ and ^{3}CDOM*, but Cermola et al. (2005) observed no photodegradation upon prolonged GFZ irradiation (up to 200 h) in the laboratory in the presence of humic acids. Because humic acids are among the natural organic matter components with the most reactive excited triplet states (Vione et al., 2014), the ^{3}CDOM* process was not considered in this work.

The studied grab natural water samples were taken from a pond (Bossea) and a mountain lake (Nivolet), located respectively in the provinces of Cuneo and Torino (NW Italy). Both samples were characterised for water absorbance (UV-vis spectrophotometry), nitrate (ion chromatography), nitrite (pre-column derivatisation with dinitrophenylhydrazine followed by liquid chromatography elution) and dissolved organic carbon (DOC, measured with a Shimadzu TOC analyser using the catalytic combustion technique). The TOC analyser was also used to determine the inorganic carbon

(IC), while pH was measured with a combined glass electrode. Further details on these characterisation techniques are reported in a previous study (De Laurentiis et al., 2012). The Bossea sample had DOC= 2 mg C L^{-1}, $[NO_3^-]$ = 20 μM, $[NO_2^-]$ = 0.06 μM, IC = 33 mg C L^{-1} and pH 8.3. The Nivolet sample had DOC= 0.6 mg C L^{-1}, $[NO_3^-]$ = 1.7 μM, $[NO_2^-]$ = 0.04 μM, IC = 15 mg C L^{-1} and pH 6.7.

GFZ spiked to Bossea and Nivolet water and to ultra-pure water to reach a 50 μM concentration underwent UVB irradiation under a Philips TL 01 lamp with emission maximum at 313 nm. The time evolution of GFZ was monitored by HPLC-UV, the transformation intermediates were identified by dichloromethane extraction followed by GC-MS analysis.

The GFZ electronic density was computed by density functional theory (DFT; Raghavachari et al., 1980; Clark et al., 1983; Foresman and Fritsch, 1996; Barone and Cossi, 1998; Marenich et al., 2009) using the quantum package Gaussian 09-A.02 (Frisch et al., 2009). The acute and chronic toxicity of the identified GFZ phototransformation intermediates was predicted by using the ECOSAR software (US-EPA, 2012). Additional details concerning the mentioned methods are provided as SM.

3. Results and Discussion

3.1. Photochemical Modelling

From preliminary model calculations we obtained that $^{\bullet}OH$ reaction and direct photolysis would strongly prevail over $^1O_2$ in GFZ photodegradation. The modelled photochemical half-life times ($t_{1/2}^{GFZ}$) in fair-weather summertime (SSD = Summer Sunny Day equivalent to 15 July at 45°N latitude) are reported in **Figure 1a** in the presence of relatively elevated nitrate and nitrite (see the

figure caption for the other water conditions). The lifetimes reach up to several months, in overall agreement with the findings of Araujo et al. (2011) under real sunlight. There is a substantial lifetime increase when increasing both the water depth *d* and the dissolved organic carbon DOC. Photochemical processes are slower in deeper water columns, the lower depths of which are scarcely illuminated by sunlight. On the other hand, high-DOC waters are rich in both dissolved organic matter (DOM) and its chromophoric fraction CDOM: DOM inhibits degradation by scavenging $^{\bullet}$OH, while CDOM competes with xenobiotics like GFZ for sunlight irradiance, thereby inhibiting their direct photolysis (Vione et al., 2014). CDOM is also a major ^{3}CDOM* source (Minella et al., 2013), but there is compelling experimental evidence against a significant triplet-sensitisation reactivity of GFZ (Cermola et al., 2005).

The values of $t_{1/2}^{GFZ}$ vs. *d* and DOC in the presence of low nitrate and nitrite levels are shown in **Figure 1b**, where the assumed concentrations of these species were one hundred times lower than for **Figure 1a**. Nitrate and nitrite are $^{\bullet}$OH sources in addition to CDOM, but their limited impact on $t_{1/2}^{GFZ}$ is further confirmed by **Figure 1c**, which reports $t_{1/2}^{GFZ}$ as a function of [NO_3^-] and [NO_2^-]. Indeed, when varying the levels of the two nitrogen species by two orders of magnitude, $t_{1/2}^{GFZ}$ was modified by a mere ~15%.

As shown in **Table 1**, there is a relatively wide variation in the literature values of the direct photolysis quantum yield Φ_{GFZ}, ranging from $1.2 \cdot 10^{-2}$ to $9.2 \cdot 10^{-2}$. The direct photolysis kinetics is linearly proportional to Φ_{GFZ}, but this is not the only pathway involved in GFZ photodegradation because the $^{\bullet}$OH process is also relevant. For this reason, a variation in Φ_{GFZ} by almost an order of magnitude causes $t_{1/2}^{GFZ}$ to vary by no more than 30-40% (see **Figure 1d**, which reports the plot of $t_{1/2}^{GFZ}$ vs. DOC and Φ_{GFZ}).

The results shown so far are referred to fair-weather summertime irradiation. The trend of $t_{1/2}^{GFZ}$ in different months of the year is shown in **Figure 2**, for intermediate values of the water depth and the DOC (5 m and 5 mg C L^{-1}, respectively) and in the two scenarios of high and low values of nitrate and nitrite. Very similar $t_{1/2}^{GFZ}$ values are predicted with either high or low nitrate and nitrite, and the $t_{1/2}^{GFZ}$ differences are always lower than the model uncertainty. The predicted GFZ half-life time is ~ two weeks in June-July, but the photodegradation is extremely limited during wintertime.

The pie charts associated to some data points in **Figure 2** give insight into the percentages of GFZ phototransformation accounted for by direct photolysis or $^{\bullet}$OH reaction. The $^{\bullet}$OH process is enhanced in the presence of elevated nitrate and nitrite, which affect the $^{\bullet}$OH reaction percentage more than they affect $t_{1/2}^{GFZ}$. The direct photolysis is enhanced during summertime, because GFZ mainly absorbs UVB radiation (see **Figure SM1**) and wintertime sunlight has a considerable UVB deficit (Frank and Klöpffer, 1988). In contrast, $^{\bullet}$OH is generated not only by nitrate that absorbs in the UVB, but also by nitrite (mostly absorbing in the UVA region) and by CDOM that absorbs UVA and visible radiation in addition to the UVB one. Therefore, $^{\bullet}$OH photoproduction is less affected by seasonal variations than the GFZ direct photolysis.

Because direct photolysis and $^{\bullet}$OH reaction are by far the main GFZ phototransformation pathways, from the fraction of photoattenuation accounted for by the direct photolysis (η_{GFZ}^{DP}) it is easy to derive the importance of the $^{\bullet}$OH process ($\eta_{GFZ}^{^{\bullet}OH}$=1-$\eta_{GFZ}^{DP}$). The modelled η_{GFZ}^{DP} is reported in **Figure 3a** (high levels of nitrate and nitrite) and in **Figure 3b** (low nitrate and nitrite levels). In both cases η_{GFZ}^{DP} decreases with increasing depth because GFZ absorbs UVB sunlight, which is efficiently scavenged by CDOM and poorly penetrates into the water column (Vione et al., 2014). The predicted η_{GFZ}^{DP} trend with DOC varies depending on the concentration levels of nitrate and nitrite that are, together with CDOM, photochemical sources of $^{\bullet}$OH (Vione et al., 2014). In the presence

of elevated nitrate and nitrite (**Figure 3a**), DOM scavenges the $^{\bullet}$OH radicals photogenerated by the two nitrogen species and inhibits the $^{\bullet}$OH process. The direct photolysis is inhibited at high DOC, too, because of competition for irradiance between GFZ and CDOM, but the $^{\bullet}$OH scavenging effect is more important in such conditions (Vione et al., 2014). Therefore, η_{GFZ}^{DP} increases with increasing DOC. With low nitrate and nitrite (**Figure 3b**), CDOM is the main $^{\bullet}$OH source and DOM the main sink (Vione et al., 2014), thus the $^{\bullet}$OH process scarcely depends on the DOC value. At elevated DOC in deep waters the main effect is the inhibition by CDOM of the GFZ direct photolysis, which explains the η_{GFZ}^{DP} decrease with increasing DOC. In contrast, at elevated DOC in shallow waters the competition for irradiance is limited and there is only a very small effect of the DOC on η_{GFZ}^{DP}, which is almost constant at around 0.8-0.9 (**Figure 3b**). From an examination of **Figures 2**, **3a** and **3b** one gets that the GFZ direct photolysis is enhanced in shallow waters during summertime, under which conditions the overall GFZ lifetime is also shorter and, therefore, photodegradation is favoured over potentially competitive attenuation pathways such as microbial transformation.

Figure 3c reports the trend of η_{GFZ}^{DP} as a function of Φ_{GFZ} and nitrite concentration. Increasing nitrite causes η_{GFZ}^{DP} to decrease to the advantage of the $^{\bullet}$OH reaction, while η_{GFZ}^{DP} increases with increasing Φ_{GFZ}. Direct photolysis and $^{\bullet}$OH reaction have a comparable weight if $\Phi_{GFZ} = 5.2 \cdot 10^{-2}$, but there would be prevalence of the direct photolysis with $\Phi_{GFZ} = 9.2 \cdot 10^{-2}$ and of the $^{\bullet}$OH process with $\Phi_{GFZ} = 1.2 \cdot 10^{-2}$.

3.2. GFZ photodegradation trend and phototransformation intermediates

The time evolution of GFZ upon UVB irradiation in Milli-Q (ultra-pure) water and in the Bossea and Nivolet natural water samples is reported in **Figure 4**. In all the cases the GFZ photodegradation followed a pseudo-first order kinetics, and degradation was faster in ultra-pure than in natural water. In the case of ultra-pure water the direct photolysis is expected to be the only

phototransformation pathway, while both direct photolysis and indirect photochemistry would account for GFZ phototransformation in natural waters. In the Bossea and Nivolet samples there should be some degree of competition for lamp irradiance between GFZ and CDOM (the main UVB absorber in natural waters; Loiselle et al., 2012), inhibiting the direct photolysis but triggering indirect phototransformation. In our case the experimental data suggest that the occurrence of indirect photochemistry could not offset the inhibition of direct photolysis. As suggested by **Figure 3**, the direct photolysis is actually expected to be the main GFZ phototransformation pathway in very shallow waters (as is typical of laboratory irradiation set-ups), with nitrate levels below 0.1 mM like in our case.

The fact that the degradation kinetics followed the order Milli-Q > Nivolet > Bossea, where the Bossea water had twice as high the 313-nm absorbance (A_{313nm}) and three times as high the DOC as the Nivolet one, may apparently suggest that competition for irradiance could play a major role in the inhibition of GFZ direct photolysis. However, by considering the 1.2-cm optical path length inside the irradiated solutions, one gets that both samples had A_{313nm} < 0.01. Therefore, CDOM could absorb less than 2% of the incident radiation in these samples and could not significantly decrease the photon flux absorbed by GFZ. The observed degradation trend could more likely derive from an interference of natural DOM over the direct photolysis pathway of GFZ, similarly to previous observations made on phenoxyacetic acid herbicides (Vione et al., 2010). In analogy with the cited work, if GFZ direct photolysis involved its excited states (e.g. the triplet ^{3}GFZ*), ^{3}GFZ* could oxidise DOM to produce a GFZ radical anion ($GFZ^{-\bullet}$) that could be recycled back to GFZ by molecular oxygen. Such a process would decrease Φ_{GFZ}, inhibiting GFZ degradation without affecting the absorbed photon flux. In the following, note that ISC = Inter-System Crossing.

$$GFZ + h\nu \rightarrow {}^1GFZ^* \xrightarrow{ISC} {}^3GFZ^* \quad (1)$$

$${}^3GFZ^* \rightarrow \text{Products} \quad (2)$$

$${}^3GFZ^* + DOM \rightarrow GFZ^{-\bullet} + DOM^{+\bullet} \quad (3)$$

$$GFZ^{-\bullet} + O_2 \rightarrow GFZ + O_2^{-\bullet} \quad (4)$$

The GC-MS data suggested the formation of at least twelve transformation intermediates (TIs) of GFZ, and the same compounds were detected in both ultra-pure and natural water. Their proposed structures, mass spectra, m/z ratios and retention times are reported in **Table SM1**. The TIs structures are also reported in **Table 2**, together with that of GFZ. In the mass spectra of several intermediates (**TI1**, **TI2**, **TI3**, **TI6**, **TI7**, **TI8**, **TI9**) the presence of a fragment at 121 m/z, also reported in the fragmentation pathway of GFZ, suggests that the phototransformation of the substrate involved the aliphatic moiety and not the aromatic one. This issue can be accounted for by the fact that the electronic density of GFZ is particularly high on the aromatic ring, on the ether oxygen, but most notably on the carboxylic function (see **Figure 5**). Therefore, the phototransformation of GFZ is most likely to start from the carboxylic group and to involve mainly the alkyl lateral chain.

Due to a limited fragmentation extent, the mass spectra of **TI2** and **TI3** are not very informative and they are consistent with either aliphatic or carbonyl structures (both options are reported in **Table 2**). However, the carbonyl structures seem more likely as they fit better into the hypothesised photodegradation pathway (*vide infra*). In the case of **TI8** and **TI9**, the two peaks eluted at 26.2 and 27.0 min, respectively. The mass spectra are consistent with the presence of an unsaturation in the aliphatic chain, which could occur in two alternative positions (C_1=C_2 or C_2=C_3, if alkyl chain numbering starts from the carbon atom that is nearest to the aromatic ring). In the presence of two alternative unsaturation positions in a non-symmetric structure one would expect the presence of two couples of *cis-trans* isomers, which is not consistent with the detection of only two peaks. Therefore, the formation of only one couple of *cis-trans* isomers seems more likely. Considering that both **TI8** and **TI9** might derive from the oxidation of **TI1** (*vide infra*), the unsaturation would likely involve C_1=C_2 as they are the couple of C atoms nearest to the ether oxygen. The electronic

density is in fact quite high on the ether function (see for instance **Figure 5**), which might favour the transformation of nearby groups.

Based on the GFZ and TIs structures and on the possible pathways that could take place during direct photodegradation, the transformation scheme reported in **Figure 6** can be tentatively proposed. The figure reports the TIs acronyms and proposed structures, the hypothesised transformation pathways, and a semi-quantitative insight into the peak areas to differentiate intense peaks from low ones. The correlation between the GC-MS peak areas and the concentrations of the relevant compounds in aqueous solution depends on several factors (extraction and ionisation efficiencies, MS sensitivity), but as a first approximation the peak areas may give some insight into the possible occurrence of major and minor intermediates. Upon sunlight absorption, GFZ could undergo decarboxylation to give **TI6** and **TI7**, which might be oxidised to produce the carbonyl-containing compounds **TI2** and **TI3**. If the hypothesis here holds that the peak areas are roughly proportional to the aqueous-phase concentrations, the fact that the **TI6** and **TI7** peaks are less intense than the **TI2** and **TI3** ones might be due to a very fast transformation of the former compounds. GFZ decarboxylation would also produce **TI1**, which might be oxidised into **TI8** and **TI9** (presumably a couple of *cis*/*trans* isomers). The presence of an unsaturation in **TI8** and **TI9** might favour further reactivity, such as the cleavage of the alkyl chain to produce **TI4** (2,5-dimethylphenol, the TI having the most intense peak) and presumably a series of C_6 compounds with 5-member rings (**TI10** to **TI12**). These compounds might be formed *via* intra-molecular processes involving the C_6 alkyl chain after or upon detachment from the aromatic ring. Similarly to many undissociated phenols (De Laurentiis et al., 2013), irradiated **TI4** could then be transformed into the corresponding phenoxy radical that would be a precursor to the substituted benzoquinone **TI5** (Zhu et al., 2007).

3.3. Model assessment of TIs acute and chronic toxicity

The potential acute and chronic toxic effects of GFZ and its identified transformation intermediates were assessed with the ECOSAR software (US-EPA, 2012). The calculation results for the various toxicity endpoints (acute and chronic values for fish, daphnid and algae) are reported in **Table 2**, which shows that GFZ, **TI1** and **TI4** have comparable and relatively low toxicity for the considered aquatic organisms. In the case of **TI2** and **TI3** the structural identification is quite important as far as toxicity is concerned, because the hydrocarbon structures would be more toxic than the carbonyl ones (Mayo-Bean et al., 2012). Considering that the occurrence of carbonyl compounds seems more likely in the context of a reasonable photodegradation pathway, the phototransformation of GFZ into **TI2** and **TI3** might not end up into compounds of toxicological concern. However, **TI6** and **TI7** that could be the immediate precursors of **TI2** and **TI3** might be significantly more toxic than GFZ. This issue could be a problem in the early transformation of GFZ, unless the low peak areas of **TI6** and **TI7** really suggest that the two compounds occur in low concentration.

TI8 and **TI9** are not expected to be particularly toxic, with the exception of a possibly significant chronic toxicity to fish, and the cleavage of the alkyl chain would produce poorly toxic compounds such as **TI4** and C_6 molecules with five-member rings (**TI10** to **TI12**). However, the further oxidation of **TI4** would produce the highly toxic quinone **TI5** that, due to a combination of expected toxicity and peak area, is a concerning intermediate of GFZ phototransformation and the most concerning one among the TIs identified in this work.

Interestingly, **TI5** is also reported to form in the reaction between GFZ and $^{\bullet}$OH (Razavi et al., 2009). Other intermediates formed in the same process are a GFZ derivative with a C=C bond in the aliphatic chain, a ring-hydroxylated derivative of the latter and some ring-hydroxylated GFZ intermediates. All these compounds are expected to show comparable toxicity as GFZ. In contrast, a $^{\bullet}$OH intermediate bearing three -OH substituents on the aromatic ring (Razavi et al., 2009) has a hydroquinone structure that could cause significant chronic toxicity to fish (ECOSAR-predicted

ChV = 70 μg L^{-1}). Other $^{\bullet}$OH intermediates are the *ortho*-benzoquinone analogue of **TI5**, which should be poorly toxic differently from the *para* compound (Mayo-Bean et al., 2012), as well as open-chain carboxylic acids derived from lateral-chain cleavage (Razavi et al., 2009). The toxicity of these compounds is expected to be very limited.

Finally, the biotransformation of GFZ causes hydroxylation of the ring methyl groups (Kang et al., 2009). According to the ECOSAR software, these compounds are expected to be considerably less toxic than GFZ itself.

Conclusions

GFZ is expected to be fairly persistent in environmental waters, with half-life times that reach up to several months under summertime conditions in relatively deep environments with elevated DOC, and practically negligible phototransformation during winter. Limited effects on the GFZ half-life times are expected in the presence of even large variations of nitrate and nitrite concentration values. The literature data for the direct photolysis quantum yield Φ_{GFZ} vary by a factor of 7-8, but such variations are strongly dampened as far as the resulting GFZ half-life times are concerned. The factors that mostly affect the photochemical half-life time of GFZ are actually water depth, DOC and season. The direct photolysis and the $^{\bullet}$OH reaction are expected to be the main phototransformation pathways of GFZ, with the direct photolysis prevailing during summertime in shallow waters with low nitrate and nitrite and the $^{\bullet}$OH process prevailing under the opposite conditions. The DOC effect on the ratio between the two processes is not substantial and it is very variable depending on water chemistry and depth. Considering that GFZ phototransformation is relatively fast in shallow waters in summertime and much slower in deep ones in winter, the direct photolysis prevails when GFZ photochemistry is more likely to overcome other attenuation

pathways (e.g. microbial degradation). Therefore, direct photolysis is expected to play a key role in GFZ photodegradation under environmental conditions.

Most of the identified GFZ phototransformation intermediates are expected to show comparable toxicity as GFZ itself. The compound that should be regarded with the highest concern is probably **TI5** (2,5-dimethyl-1,4-benzoquinone), which is also formed upon reaction between GFZ and $^{\bullet}$OH.

Acknowledgements

Financial support by MIUR-PNRA is gratefully acknowledged.

References

Andreozzi, R., Marotta, R., Paxéus, N., 2003. Pharmaceuticals in STP effluents and their solar photodegradation in aquatic environment. Chemosphere 50, 1319-1330.

Araujo, L., Villa, N., Camargo, N., Bustos, M., Garcia, T., Prieto, A. d. J., 2011. Persistence of gemfibrozil, naproxen and mefenamic acid in natural waters. Environ. Chem. Lett. 9, 13-18.

Barone, V., Cossi, M., 1998. Quantum calculation of molecular energies and energy gradients in solution by a conductor solvent model. J. Phys. Chem. A 102, 1995-2001.

Bodrato, M., Vione, D., 2014. APEX (Aqueous Photochemistry of Environmentally occurring Xenobiotics): A free software tool to predict the kinetics of photochemical processes in surface waters. Environ. Sci.: Processes Impacts 16, 732-740.

Boreen, A. L., Arnold, W. A., McNeill, K., 2003. Photodegradation of pharmaceuticals in the aquatic environment: A review. Aquat. Sci. 65, 320-341.

Canonica, S., Kohn, T., Mac, M., Real, F.J., Wirz, J., von Gunten, U., 2005. Photosensitizer method to determine rate constants for the reaction of carbonate radical with organic compounds. Environ. Sci. Technol. 39, 9182-9188.

Cermola, M., DellaGreca, M., Iesce, M. R., Previtera, L, Rubino, M., Temussi, F., Brigante, M., 2005. Phototransformation of fibrate drugs in aqueous media. Environ. Chem. Lett. 3, 43-47.

Clark, T., Chandrasekhar, J., Spitznagel, G. W., Schleyer, P. V. R., 1983. Efficient diffuse function-augmented basis sets for anion calculations. III. The 3-21+G basis set for first-row elements, Li–F. J. Comput. Chem. 4, 294-301.

D'Alessio, M., Yoneyama, B., Kirs, M., Kisand, V., Ray, C., 2015. Pharmaceutically active compounds: Their removal during slow sand filtration and their impact on slow sand filtration bacterial removal. Sci. Total Environ. 524, 124-135.

De Laurentiis, E., Minella, M., Maurino, V., Minero, C., Brigante, M., Mailhot, G., Vione, D., 2012. Photochemical production of organic matter triplet states in water samples from mountain lakes, located below or above the tree line. Chemosphere, 88, 1208-1213.

De Laurentiis, E., Minella, M., Sarakha, M., Marrese, A., Minero, C., Mailhot, G., Brigante, M., Vione, D., 2013. Photochemical processes involving the UV absorber benzophenone-4 (2-hydroxy-4-methoxybenzophenone-5-sulphonic acid) in aqueous solution: Reaction pathways and implications for surface waters. Water Res. 47, 5943-5953.

Foresman, J. B., Frisch, Æ, 1996. Exploring Chemistry with Electronic Structure Methods. Gaussian, Inc., Pittsburgh, PA, pp. 166-168.

Frank, R., Klöpffer, W., 1988. Spectral solar photo irradiance in Central Europe and the adjacent north Sea, Chemosphere 17, 985-994.

Frisch, M. J., Trucks, G. W., Schlegel, H. B., Scuseria, G. E., Robb, M. A., Cheeseman, J. R., Scalmani, G., Barone, V., Mennucci, B., Petersson, G. A., Nakatsuji, H., Caricato, M., Li, X., Hratchian, H. P., Izmaylov, A. F., Bloino, J., Zheng, G., Sonnenberg, J. L., Hada, M., Ehara, M., Toyota, K., Fukuda, R., Hasegawa, J., Ishida, M., Nakajima, T., Honda, Y., Kitao, O.,

Nakai, H., Vreven, T., Montgomery Jr., J. A., Peralta, J. E., Ogliaro, F., Bearpark, M., Heyd, J. J., Brothers, E., Kudin, K. N., Staroverov, V. N., Kobayashi, R., Normand, J., Raghavachari, K., Rendell, A., Burant, J. C., Iyengar, S. S., Tomasi, J., Cossi, M., Rega, N., Millam, J. M., Klene, M., Knox, J. E., Cross, J. B., Bakken, V., Adamo, C., Jaramillo, J., Gomperts, R., Stratmann, R. E., Yazyev, O., Austin, A. J., Cammi, R., Pomelli, C., Ochterski, J. W., Martin, R. L., Morokuma, K., Zakrzewski, V. G., Voth, G. A., Salvador, P., Dannenberg, J. J., Dapprich, S., Daniels, A. D., Farkas, Ö., Foresman, J. B., Ortiz, J. V., Cioslowski, J., Fox, D. J., 2009. Gaussian 09, Gaussian, Inc., Wallingford, CT.

Gligorovski, S., Strekowski, R., Barbati, S., Vione, D., 2015. Environmental implications of hydroxyl radicals ($^{\bullet}$OH). Chem. Rev. 115, 13051-13092.

HealthGrove, 2016. *http://drugs.healthgrove.com/l/778/Gemfibrozil*, last accessed June 2016.

Isidori, M., Nardelli, A., Pascarella, L., Rubino, M., Parrella, A., 2007. Toxic and genotoxic impact of fibrates and their photoproducts on non-target organisms. Environ. Int. 33, 635-641.

Kang, S. I., Kang, S. Y., Kanaly, R. A., Lee, E., Lim, Y., Hur, H. G., 2009. Rapid oxidation of ring methyl groups is the primary mechanism of biotransformation of gemfibrozil by the fungus *Cunninghamella elegans*. Arch. Microbiol. 191, 509-517.

Krkosek, W. H., Peldszus, S., Huck, P. M., Gagnon, G. A., 2014. Formation kinetics of gemfibrozil chlorination reaction products: Analysis and application. Water Environ. Res. 86, 654-662.

Loiselle, S., Vione, D., Minero, C., Maurino, V., Tognazzi, A., Dattilo, A. M., Rossi, C., Bracchini, L., 2012. Chemical and optical phototransformation of dissolved organic matter. Water Res. 46, 3197-3207.

Ma, J. S., Lv, W. Y., Chen, P., Lu, Y., Wang, F. L., Li, F., Yao, K., Liu, G. G., 2016. Photodegradation of gemfibrozil in aqueous solution under UV irradiation: kinetics, mechanism, toxicity, and degradation pathways. Environ. Sci. Pollut. Res. 23, 14294-14306.

Marenich, A. V., Cramer, C. J., Truhlar, D. G., 2009. Universal solvation model based on solute electron density and on a continuum model of the solvent defined by the bulk dielectric constant and atomic surface tensions. J. Phys. Chem. B 113, 6378-6396.

Mayo-Bean, K., Moran, K., Meylan, B., Ranslow, P., 2012. Methodology Document for the ECOlogical Structure-Activity Relationship Model (ECOSAR) Class Program. US-EPA, Washington DC, 46 pp.

Minella, M., De Laurentiis, E., Buhvestova, O., Haldna, M., Kangur, K., Maurino, V., Minero, C., Vione, D., 2013. Modelling lake-water photochemistry: three-decade assessment of the steady-state concentration of photoreactive transients ($^{\bullet}OH$, $CO_3^{-\bullet}$ and $^3CDOM^*$) in the surface water of polymictic Lake Peipsi (Estonia/Russia). Chemosphere 90, 2589-2596.

Minella, M., De Laurentiis, E., Maurino, V., Minero, C., Vione, D., 2015. Dark production of hydroxyl radicals by aeration of anoxic lake water. Sci. Total Environ. 527-528, 322-327.

Osorio, V., Larranaga, A., Acena, J., Perez, S., Barcelo, D., 2016. Concentration and risk of pharmaceuticals in freshwater systems are related to the population density and the livestock units in Iberian Rivers. Sci. Total Environ. 540, 267-277.

Page, S. E., Arnold, W. A., McNeill, K., 2011. Assessing the contribution of free hydroxyl radical in organic matter-sensitized photohydroxylation reactions. Environ. Sci. Technol. 45, 2818-2825.

Raghavachari, K., Binkley, J. S., Seeger, R., Pople, J. A., 1980. Self-consistent molecular orbital methods. XX. A basis set for correlated wave functions. J. Chem. Phys. 72, 650-654.

Razavi, B., Song, W. H., Cooper, W. J., Greaves, J., Jeong, J., 2009. Free-radical-induced oxidative and reductive degradation of fibrate pharmaceuticals: Kinetic studies and degradation mechanisms. J. Phys. Chem. A 113, 1287-1294.

Rogora, M., Colombo, L., Lepori, F., Marchetto, A., Steingruber, S., Tornimbeni, O., 2013. Thirty years of chemical changes in acid-sensitive lakes in the Alps. Water Air Soil Pollut. 224, 1746.

Shu, Z., Bolton, J. R., Belosevic, M., Gamal El Din, M., 2013. Photodegradation of emerging micropollutants using themedium-pressure UV/H_2O_2 Advanced Oxidation Process. Water Res. 47, 2881-2889.

Sucker, C., Krause, K., 2010. Increasing dissolved organic carbon concentrations in freshwaters: What is the actual driver? iForest 3, 106-108.

US-EPA, 2012. *https://www.epa.gov/tsca-screening-tools/ecological-structure-activity-relationships-ecosar-predictive-model*, last accessed November 2016.

Vione, D., Khanra, S., Das, R., Minero, C., Maurino, V., Brigante, M., Mailhot, G., 2010. Effect of dissolved organic compounds on the photodegradation of the herbicide MCPA in aqueous solution. Water Res. 44, 6053-6062.

Vione, D., Minella, M., Maurino, V., Minero, C., 2014. Indirect photochemistry in sunlit surface waters: Photoinduced production of reactive transient species. Chem.-Eur. J. 20, 10590-10606.

Wenk, J., Eustis, S. N., McNeill, K., Canonica, S., 2013. Quenching of excited triplet states by dissolved natural organic matter. Environ. Sci. Technol. 27, 12802-12810.

Yu, H.-W., Anumol, T., Park, M., Pepper, I., Scheideler, J., Snyder, S. A., 2015. On-line sensor monitoring for chemical contaminant attenuation during UV/H_2O_2 advanced oxidation process. Water Res. 81, 250-260.

Yurdakal, S., Loddo, V., Augugliaro, V., Berber, H., Palmisano, G., Palmisano, L., 2007. Photodegradation of pharmaceutical drugs in aqueous TiO_2 suspensions: Mechanism and kinetics. Catal. Today 129, 9-15.

Zhu, B. Z, Kalyanaraman, B., Jiang, G. B., 2007. Molecular mechanism for metal-independent production of hydroxyl radicals by hydrogen peroxide and halogenated quinones. Proc. Natl. Acad. Sci. USA 104, 17575-17578.

Table 1. Photochemical parameters (direct photolysis quantum yields and second-order reaction rate constants) of GFZ phototransformation, as derived from the literature (the relevant literature reference is provided near each reported value). The values used in this work (averages of literature values where relevant) are also provided.

Photochemical parameters	***Parameter values***	***References***	***Used value (average where applicable)***
Φ_{GFZ}, unitless	$1.2 \cdot 10^{-2}$	Isidori et al., 2007	$5.2 \cdot 10^{-2}$ (unless otherwise specified)
	$9.2 \cdot 10^{-2}$	Yu et al., 2015	
$k_{GFZ,^{\bullet}OH}$, L mol^{-1} s^{-1}	$1.0 \cdot 10^{10}$	Razavi et al., 2009	$8.6 \cdot 10^{9}$
	$9.1 \cdot 10^{9}$	Yu et al., 2015	
	$6.8 \cdot 10^{9}$	Shu et al., 2013	
$k_{GFZ,^1O_2}$, L mol^{-1} s^{-1}	$2.6 \cdot 10^{6}$	Ma et al., 2016	$2.6 \cdot 10^{6}$

Table 2. Acute (LC50, EC50) and chronic (ChV) toxicity towards aquatic organisms of GFZ and its transformation intermediates, assessed with the ECOSAR software. Values around or lower than 0.15 mg L^{-1} are expressed in µg L^{-1} units and are highlighted in bold italics. Alternative structures are shown for **TI2**, **TI3**, **TI8** and **TI9**.

	LC50 Fish (96h)	**LC50 Daphnid (48h)**	**EC50 Green algae (96 h)**	**ChV Fish**	**ChV Daphnid**	**ChV Green algae**
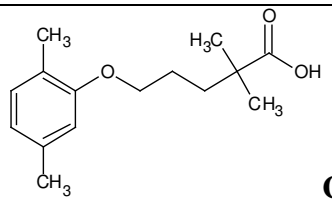 **GFZ**	6.7 mg L^{-1}	4.9 mg L^{-1}	11 mg L^{-1}	0.9 mg L^{-1}	1.0 mg L^{-1}	4.9 mg L^{-1}
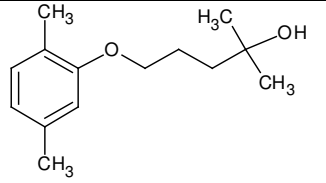 **TI1**	2.6 mg L^{-1}	1.8 mg L^{-1}	3.0 mg L^{-1}	0.3 mg L^{-1}	0.3 mg L^{-1}	1.2 mg L^{-1}
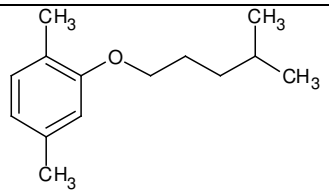	***110 µg L^{-1}***	***87 µg L^{-1}***	0.25 mg L^{-1}	***16 µg L^{-1}***	***21 µg L^{-1}***	***140 µg L^{-1}***
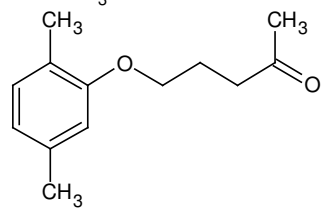 **TI2**	18 mg L^{-1}	11 mg L^{-1}	13 mg L^{-1}	2.0 mg L^{-1}	1.5 mg L^{-1}	4.2 mg L^{-1}
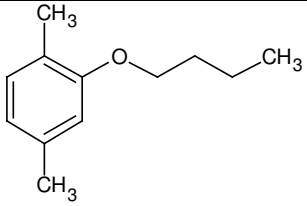	0.62 mg L^{-1}	0.45 mg L^{-1}	0.92 mg L^{-1}	***80 µg L^{-1}***	***90 µg L^{-1}***	0.41 mg L^{-1}
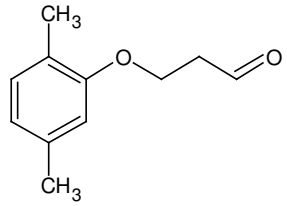 **TI3**	4.6 mg L^{-1}	5.3 mg L^{-1}	9.4 mg L^{-1}	0.54 mg L^{-1}	0.88 mg L^{-1}	3.9 mg L^{-1}
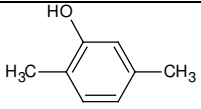 **TI4**	7.3 mg L^{-1}	2.9 mg L^{-1}	13 mg L^{-1}	0.8 mg L^{-1}	0.6 mg L^{-1}	5.8 mg L^{-1}
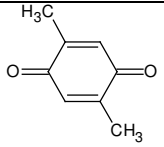 **TI5**	***70 µg L^{-1}***	0.37 mg L^{-1}	***46 µg L^{-1}***	***6 µg L^{-1}***	1.4 mg L^{-1}	***11 µg L^{-1}***
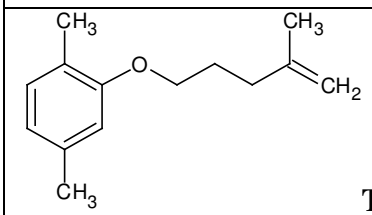 **TI6**	***110 µg L^{-1}***	***87 µg L^{-1}***	0.25 mg L^{-1}	***16 µg L^{-1}***	***21 µg L^{-1}***	***140 µg L^{-1}***

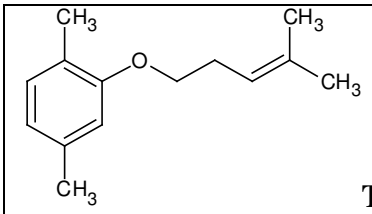 **TI7**	***130 µg L^{-1}***	***100 µg L^{-1}***	0.28 mg L^{-1}	***18 µg L^{-1}***	***24 µg L^{-1}***	***151 µg L^{-1}***
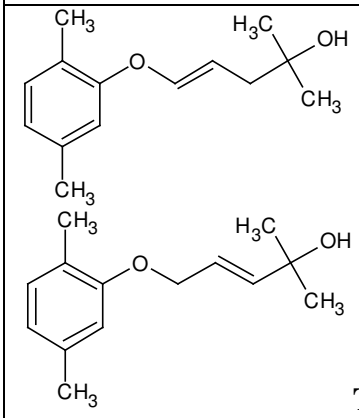 **TI8, TI9**	0.75 mg L^{-1}	1.3 mg L^{-1}	1.6 mg L^{-1}	***15 µg L^{-1}***	0.39 mg L^{-1}	0.82 mg L^{-1}
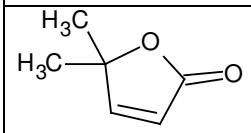 **TI10**	140 mg L^{-1}	340 mg L^{-1}	190 mg L^{-1}	15 mg L^{-1}	380 mg L^{-1}	28 mg L^{-1}
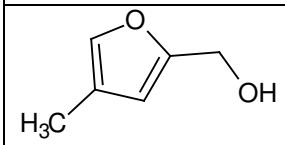 **TI11**	260 mg L^{-1}	190 mg L^{-1}	57 mg L^{-1}	19 mg L^{-1}	25 mg L^{-1}	22 mg L^{-1}
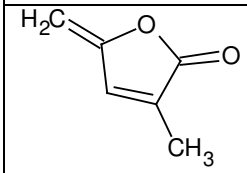 **TI12**	260 mg L^{-1}	190 mg L^{-1}	0.48 mg L^{-1}	25 mg L^{-1}	17 mg L^{-1}	0.27 mg L^{-1}

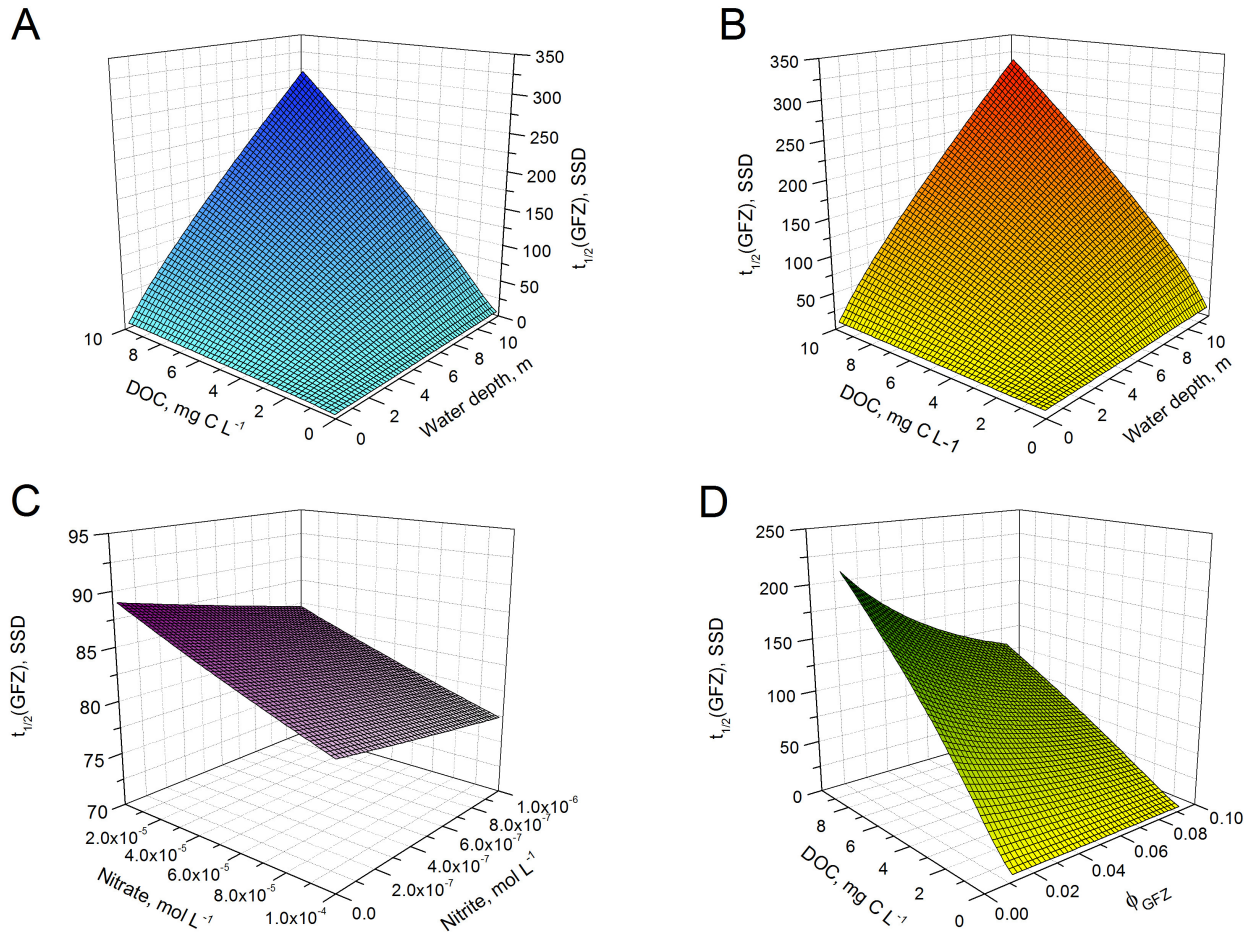

Figure 1. **(a)** GFZ half-life time (SSD = summer sunny days) for photochemical transformation, as a function of the water depth *d* and of the DOC, in the presence of 0.1 mmol L^{-1} NO_3^-, 1 µmol L^{-1} NO_2^-, 2 mmol L^{-1} HCO_3^- and 10 µmol L^{-1} CO_3^{2-}. $\Phi_{GFZ} = 5.2 \cdot 10^{-2}$.

(b) GFZ half-life time (SSD = summer sunny days) for photochemical transformation, as a function of the water depth *d* and of the DOC, in the presence of 1 µmol L^{-1} NO_3^-, 10 nmol L^{-1} NO_2^-, 2 mmol L^{-1} HCO_3^- and 10 µmol L^{-1} CO_3^{2-}. $\Phi_{GFZ} = 5.2 \cdot 10^{-2}$.

(c) GFZ half-life time for photochemical transformation, as a function of the concentration values of nitrate and nitrite, in the presence of 5 mg C L^{-1} DOC, 2 mmol L^{-1} HCO_3^- and 10 µmol L^{-1} CO_3^{2-}, for a water depth $d = 5$ m. $\Phi_{GFZ} = 5.2 \cdot 10^{-2}$.

(d) GFZ half-life time for photochemical transformation, as a function of the water DOC and of the direct photolysis quantum yield Φ_{GFZ}, in the presence of 0.1 mmol L^{-1} NO_3^-, 1 µmol L^{-1} NO_2^-, 2 mmol L^{-1} HCO_3^- and 10 µmol L^{-1} CO_3^{2-}, for a water depth $d = 5$ m.

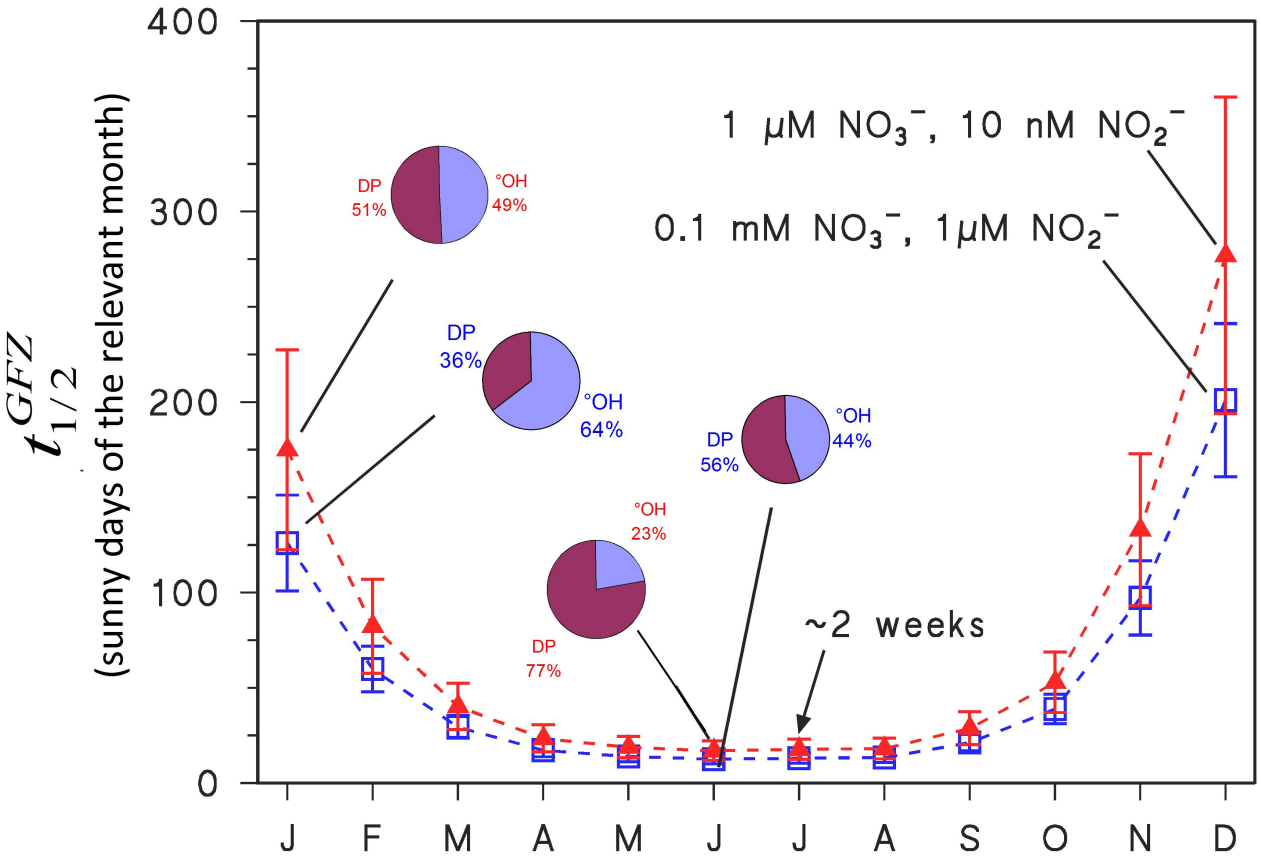

Figure 2. Monthly trend of the half-life time of GFZ, in the presence of relatively elevated (blue square symbols) or low (red triangular symbols) nitrate and nitrite concentration values. Other water conditions: 5 mg C L^{-1} DOC, 2 mmol L^{-1} HCO_3^-, 10 μmol L^{-1} CO_3^{2-}, water depth d = 5 m. Moreover, Φ_{GFZ} = $5.2 \cdot 10^{-2}$. Note that $t_{1/2}^{GFZ}$ ~ 2 weeks in the summer season, independently of the nitrate/nitrite levels. The pie charts show the percentages of GFZ phototransformation accounted for by direct photolysis and $^{\bullet}OH$ reaction in the different conditions (the blue font refers to high nitrate and nitrite, the red font to low nitrate and nitrite). The error bounds represent the σ-level uncertainties in model predictions.

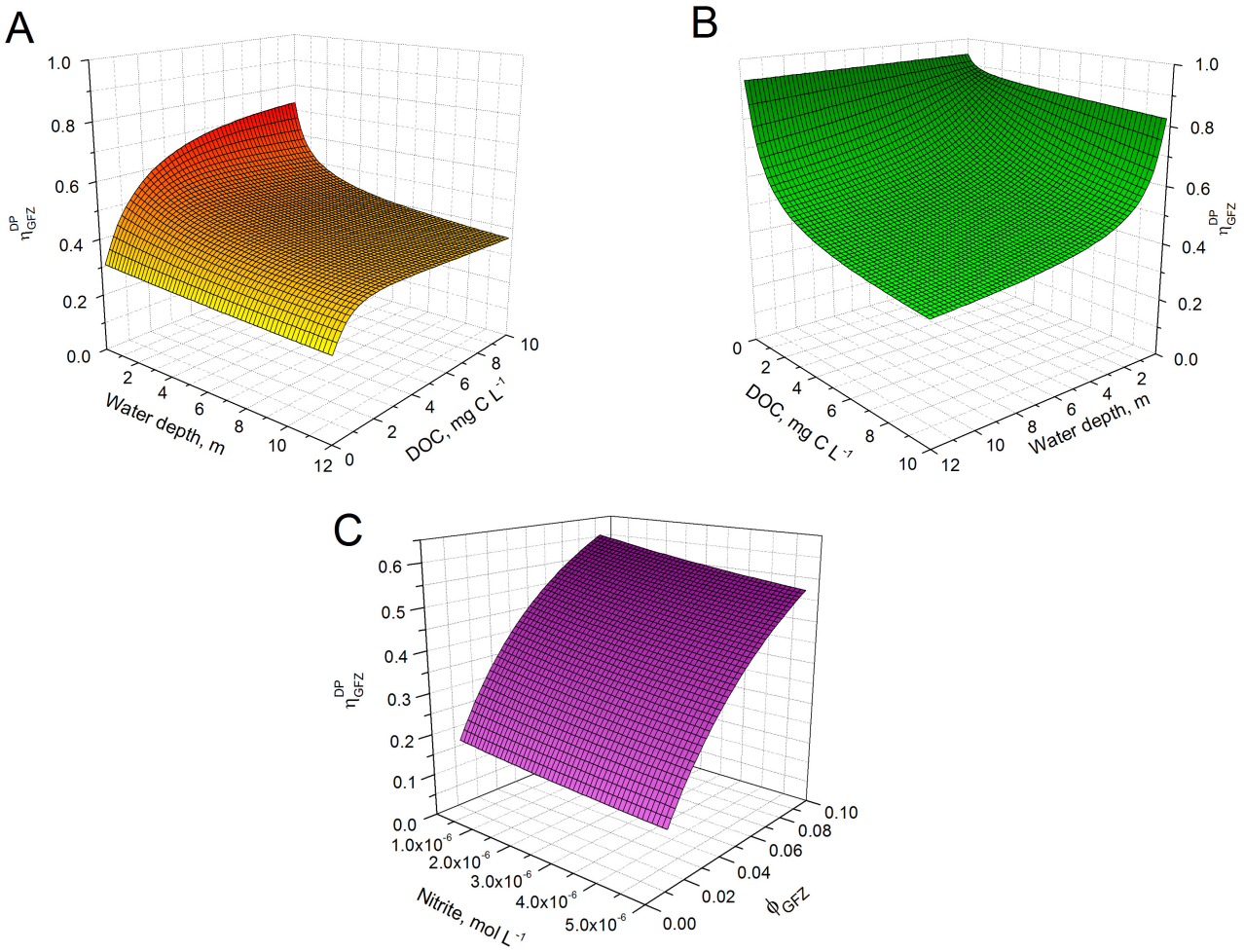

Figure 3. **(a)** Fraction of GFZ phototransformation accounted for by direct photolysis (η_{GFZ}^{DP}), as a function of d and DOC, in the presence of 2 mmol L^{-1} HCO_3^-, 10 µmol L^{-1} CO_3^{2-}, 0.1 mmol L^{-1} NO_3^- and 1 µmol L^{-1} NO_2^-. $\Phi_{GFZ} = 5.2 \cdot 10^{-2}$.

(b) Same as before, but with 1 µmol L^{-1} NO_3^- and 10 nmol L^{-1} NO_2^-.

(c) Values of η_{GFZ}^{DP} as a function of Φ_{GFZ} and nitrite concentration, in the presence of 5 mg C L^{-1} DOC, 2 mmol L^{-1} HCO_3^-, 10 µmol L^{-1} CO_3^{2-} and 0.1 mmol L^{-1} NO_3^-, for a water depth d = 5 m.

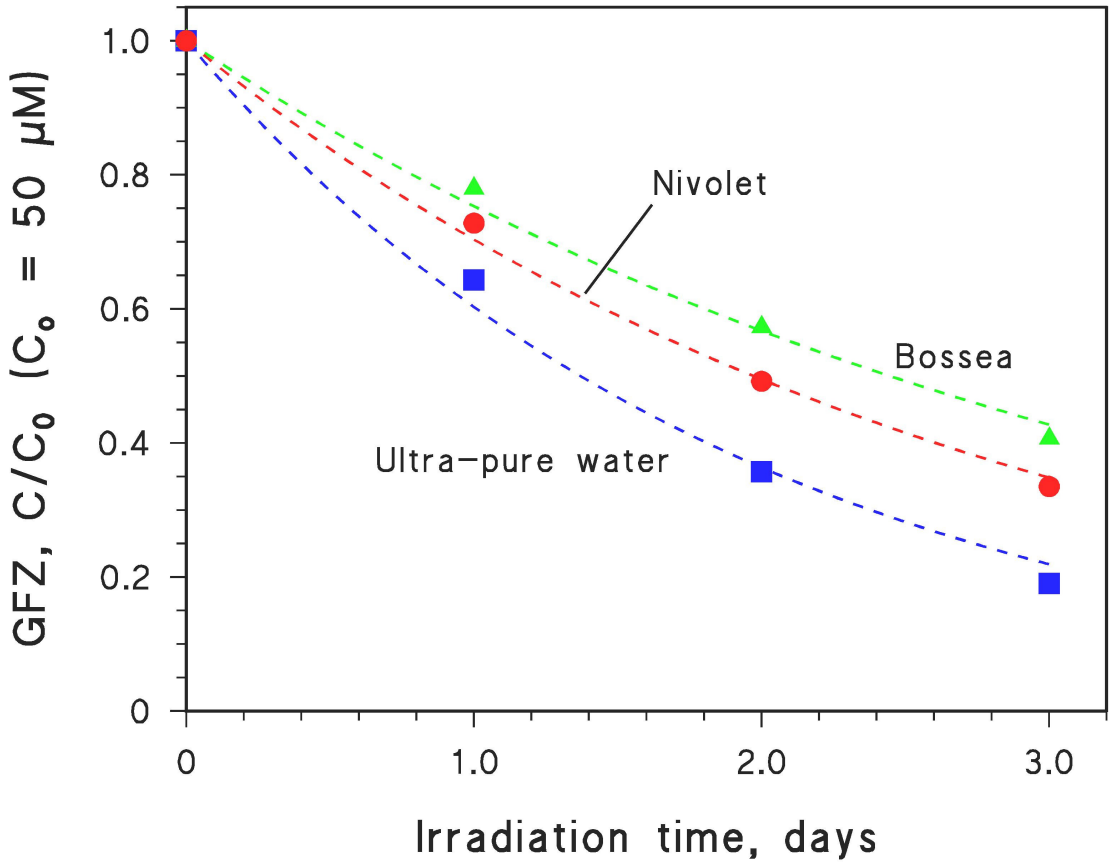

Figure 4. Time evolution of GFZ normalised concentration (C/C_o, where C_o = 50 µM is the initial GFZ concentration) upon UVB irradiation (under the 20 W Philips TL 01 lamp) in ultra-pure (Milli-Q) water as well as in two natural water samples (Bossea and Nivolet). The dashed curves represent the data fit with the equation $C/C_o = e^{-kt}$, where k is the pseudo-first order transformation rate constant and t is the irradiation time. The initial pH was 8.3 (Bossea), 6.7 (Nivolet) and 7 (Milli-Q).

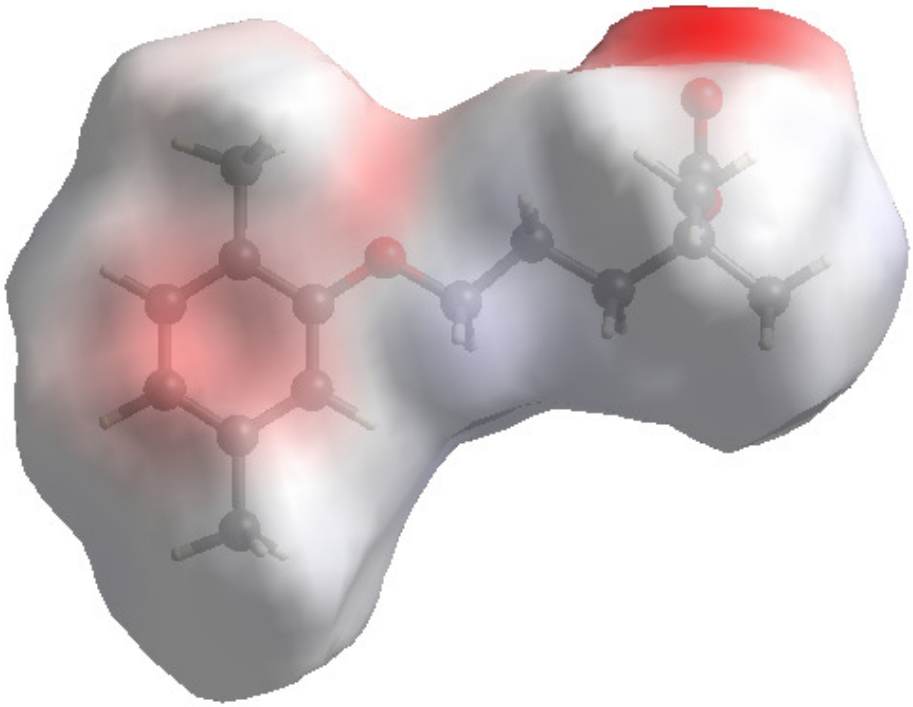

Figure 5. DFT-derived electronic density of GFZ. The regions where the electron density is the highest are highlighted in red (aromatic ring, ether oxygen and, most notably, the carboxylic group).

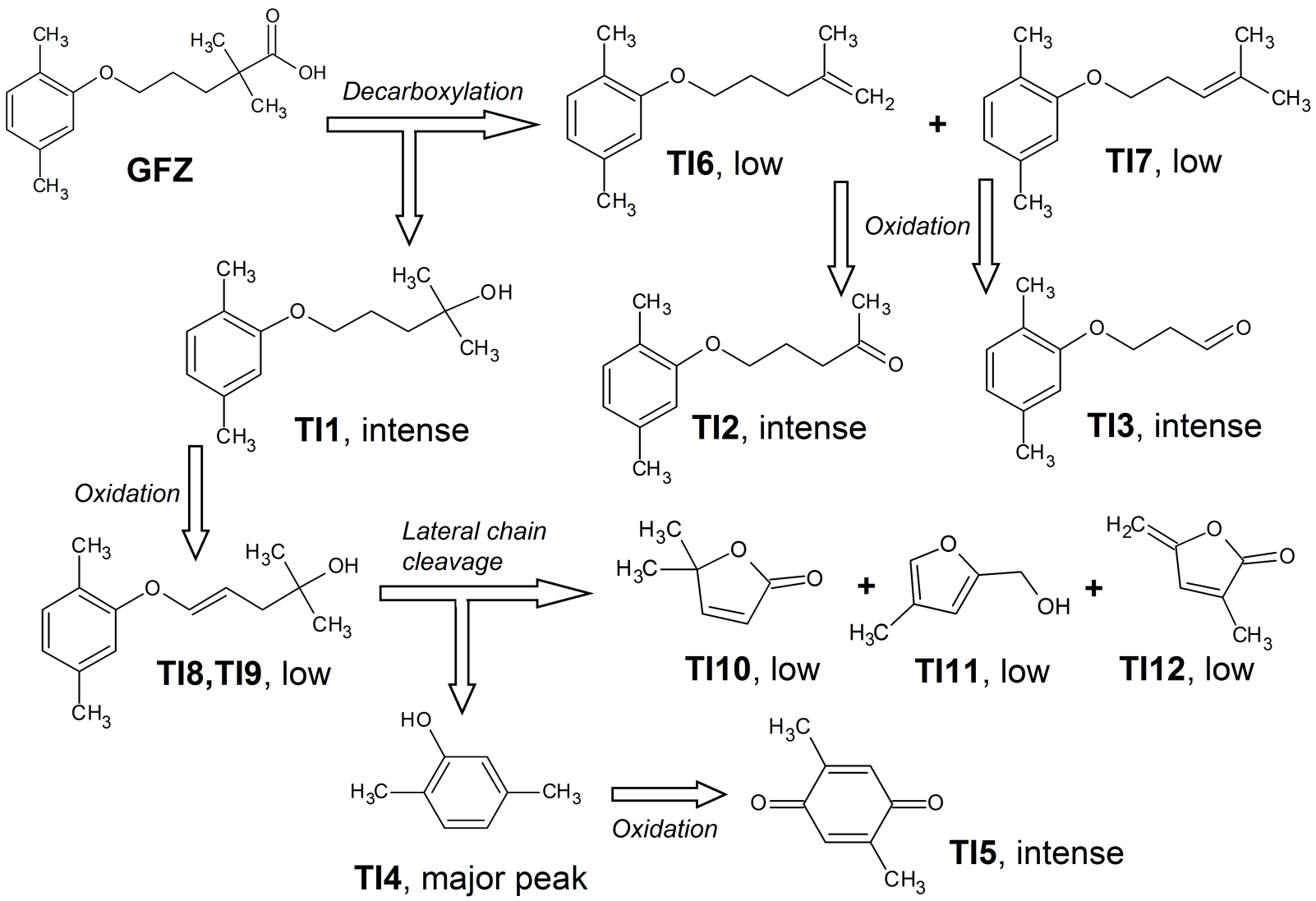

Figure 6. Tentative pathways for GFZ direct photolysis, accounting for the detected phototransformation intermediates.